coatings

MDPI

Article

Spin Coating Immobilisation of C-N-TiO_2 Co-Doped Nano Catalyst on Glass and Application for Photocatalysis or as Electron Transporting Layer for Perovskite Solar Cells

Emile Salomon Massima Mouele [1,*], Siphelo Ngqoloda [2], Sara Pescetelli [3], Aldo Di Carlo [3,4], Mihaela Dinu [5], Alina Vladescu [5,6], Anca Constantina Parau [5], Antonio Agresti [3,4], Mariana Braic [5], Christopher J. Arendse [2] and Leslie Felicia Petrik [1,*]

1 Environmental Nano Science (ENS) research group, Department of Chemistry, University of the Western Cape, Cape Town 7535, South Africa
2 Department of Physics & Astronomy, University of the Western Cape, Cape Town 7535, South Africa; sngqoloda@gmail.com (S.N.); cjarendse@uwc.ac.za (C.J.A.)
3 CHOSE, Electronic Engineering Department University of Rome Tor Vergata, Via del Politecnico 1, 00133 Rome, Italy; pescetel@uniroma2.it (S.P.); aldo.dicarlo@uniroma2.it (A.D.C.); antonio.agresti@uniroma2.it (A.A.)
4 LASE, National University of Science and Technology "MISiS", Leninsky Ave. 6, Moscow 119049, Russia
5 Research Center for Advanced Surface Processing and Analysis by Vacuum Technologies (ReCAST), National Institute for Optoelectronics (INOE) 2000, 409 Atomistilor St., Magurele, 077125 Bucharest, Romania; mihaela.dinu@inoe.ro (M.D.); alinava@inoe.ro (A.V.); anca.parau@inoe.ro (A.C.P.); mariana.braic@inoe.ro (M.B.)
6 Physical Materials Science and Composite Materials Centre, Research School of Chemistry & Applied Biomedical Sciences, Tomsk Polytechnic University, Lenin's Avenue 30, 634050 Tomsk, Russia
* Correspondence: emilemassima@yahoo.fr (E.S.M.M.); lpetrik@uwc.ac.za (L.F.P.); Tel.: +27-78-8513087 (E.S.M.M.); +27-21-9593304 (L.F.P.)

Received: 28 August 2020; Accepted: 18 October 2020; Published: 26 October 2020

Abstract: Producing active thin films coated on supports resolves many issues of powder-based photo catalysis and energy harvesting. In this study, thin films of C-N-TiO_2 were prepared by dynamic spin coating of C-N-TiO_2 sol-gel on glass support. The effect of spin speed and sol gel precursor to solvent volume ratio on the film thickness was investigated. The C-N-TiO_2-coated glass was annealed at 350 °C at a ramping rate of 10 °C/min with a holding time of 2 hours under a continuous flow of dry N_2. The C-N-TiO_2 films were characterised by profilometry analysis, light microscopy (LM), and scanning electron microscopy (SEM) coupled with energy dispersive spectroscopy (EDS). The outcomes of this study proved that a spin coating technique followed by an annealing process to stabilise the layer could be used for immobilisation of the photo catalyst on glass. The exposure of C-N-TiO_2 films to UV radiation induced photocatalytic decolouration of orange II (O.II) dye. The prepared C-N-TiO_2 films showed a reasonable power conversion efficiency average (PCE of 9%) with respect to the reference device (15%). The study offers a feasible route for the engineering of C-N-TiO_2 films applicable to wastewater remediation processes and energy harvesting in solar cell technologies.

Keywords: thin film; spin coating; immobilisation; film thickness; photocatalytic decolouration; energy harvesting; perovskite solar cells

1. Introduction

The accumulation of recalcitrant organic pollutants (ROPs) in transfer water sources has raised various questions on the safety of potable water used for drinking, households, and other activities [1,2]. Traditional mechanical, biological, physical, and chemical methods such as flocculation, coagulation, reverse osmosis, filtration, ultrafiltration, adsorption, and active sludge treatment methods have failed to remove these xenobiotic compounds from water [3]. This is because the methods listed above often transform contaminants from one phase to another instead of degrading the toxins. Also, the post-treatment of by-products resulting from these methods is costly [4].

Besides, this new generation of contaminants is present in nanogram quantities and conventional techniques have not been designed to remove these low levels of different types of pollutants, which consequently pass through the treatment processes and end up in effluents at minute concentrations [3]. Advanced oxidation processes (AOPs) were developed in recent years for the complete removal of ROPs [5,6]. AOPs are based on the production of non-selective hydroxyl radicals (OH·) [7]. After fluorine (3.06 V), the OH· radicals are considered to be the most powerful oxidant species (2.8 V) that can directly or indirectly mineralize these pollutants into dissolved CO_2, H_2O, and harmless end-products [8–10].

Among various AOPs highlighted in the literature, heterogeneous photo catalysis was identified as a robust process that can decompose and mineralize most recalcitrant contaminants [11,12]. The degradation process is induced by UV or solar light illumination of powder TiO_2 in an aqueous medium [13]. Indeed, TiO_2 is considered as a suitable semiconductor often acting as a dye-sensitizer inducing light redox-processes because of its electronic arrangement of metal atoms combined with other elements [13]. Besides, TiO_2 was found to be efficient, highly photoactive, biologically and chemically inert, inexpensive, resistant to photo corrosion and chemical corrosion, recyclable, and with a suitable band gap (E_g = 3.2 eV) suitable for oxidation and reduction processes [14,15]. These characteristics have rendered TiO_2 a popular heterogeneous semiconductor catalyst for diverse environmental applications [14,15].

In most photocatalytic applications, TiO_2 powder is dispersed in an aqueous solution to induce the photocatalytic process [16]. However, the suspension of TiO_2 powder in aqueous media may result in high filtration costs to remove the suspended TiO_2 particles [17]. This in turn represents a limitation from an industrial perspective. The immobilization of TiO_2 on diverse supports has been suggested as a palliative solution to overcome this limitation [18]. From this point of view, TiO_2 was immobilized on various supports including glass, glass beads, quartz, silica, activated carbon, fiber glass cloth, zeolites, stainless steel, ceramics, cloth, monolith, polymers, and membranes [19]. The decrease of the TiO_2 surface area was identified as the principal disadvantage during its deposition on the aforementioned supports [19,20].

Several methods, including chemical vapor deposition, electron beam evaporation, reactive magnetron sputtering, spray pyrolysis, electrophoresis, cathodic arc evaporation (CAE), reactive thermal deposition, static-dynamic films compressed, and sol-gel methods were used for immobilization of TiO_2 on supports [21,22]. Likewise, the sol-gel procedure was considered as a suitable coating technique because it offers benefits such as composition controllability and the use of low-cost equipment. Preparation of films with a large surface area and high photocatalytic activity offer the possibility to engineer excellent homogenous nano-thin films of desired layers [19,23,24]. Modified TiO_2 nano composites were used as coating layers on various supports and exceptional results have been achieved. For instance, Hui Shu et al. [25] studied the protection of stone-built cultural heritage by brushing TiO_2-modified sol coating material (TSCM) and pure TiO_2 sol (p-sol). The protective properties of TSCM were assessed by various analyses including water absorption, water vapor permeability, acid resistance, and weather resistance. Their outcomes showed that good water absorption and water vapor permeability, strong acid resistance, and higher weather resistance were observed with TSCM compared to p-sol. The authors claimed their results offer valuable alternatives in protecting stone-built cultural heritage. A comparable investigation was carried out by Anara Molkenova et al. [26] who

established a practical process of producing transparent TiO_x and metal doped TiO_x thin films and their immobilization on glass supports. The authors showed that the fabricated TiO_x thin films considerably diminished the transmittance of harmful UV radiation and could therefore be beneficial for the preservation of photovoltaic appliances. Besides, they further reported that translucent and luminous TiO_x thin films could be used as security labeling systems.

During the preparation of thin films, the sol-gel method is often applied with other techniques such as spin-coating technique used to spread thin films evenly on flat supports. In this process, an excess quantity of the precursor solution is placed on the support surface. Thereafter, the support rotates at a fixed speed to spread the gel by centrifugal force and creates wet thin layers. However, a few factors, mainly the rotation speed, concentration/viscosity of the gel, and the evaporation rate to some extent may affect the thickness of the obtained films. The developed films could be used for various applications such as photo catalysis and as charge transport layers in new generation solar cells.

Therefore, in the current study, C-N-TiO_2 synthesized by a sol-gel method was spin coated on glass (borosilicate) and thermally annealed under controlled conditions. The effects of spin coating parameters such as spin speed and solution viscosity on the thickness of the prepared C-N-TiO_2 films were investigated. Thereafter, the stability and efficiency of the annealed films were tested in harsh acidic media by photocatalytic removal of O.II at the applied conditions and as an electron transporting layer for perovskite solar cells, respectively.

2. Materials and Methods

G3P-8 SPINCOAT (Specialty Coating Systems Inc. Indianapolis, IN, USA) was used for spin coating, a Brother XD-1600MT Three Zones Tube Furnace (Zhengzhou Brother Furnace Co., LTD, Zhengzhou, China) was used for thermal annealing, and Veeco DekTak 6M stylus profiler (Veeco Instruments, Inc. Tucson, AZ, USA) was used to measure the thickness of the thin films. Photo catalysis experiments were conducted with a UV lamp (Mega-Ray 160 W/240 V MR160 SPL11/14 from Kimix, Cape Town, South Africa). Polyacrylonitrile (PAN) powder (99.5%, Good fellow, Huntingdon, UK), titanium tetrachloride (M_W 189.68 g/mol), and titanium (IV) oxide (powder) Degussa (99.5%, Sigma Aldrich, Johannesburg, South Africa), N, N dimethyl formamide (DMF) 99% and ammonium nitrate (NH_4NO_3), ACS 95% (Industrial Analytical (Pty), Johannesburg, South Africa), sulfuric acid 98% and sodium hydroxide flakes CP 97% (Kimix), and Orange II sodium salt (85%, Sigma Aldrich, Johannesburg, South Africa) were used for the preparation of carbon-nitrogen co-doped gel (C-N-TiO_2) and in the photocatalytic degradation of orange II dye purchased from Kimix.

2.1. Preparation of C-N-TiO_2 Sol-Gel

Eight grams of polyacrylonitrile (PAN) were weighed and mixed with 100 mL of 99% N,N-dimethylformamide (DMF) in a 200-mL capped borosilicate glass bottle and stirred for 24 h at room temperature. Approximately 1.5 to 3 mL of 98% concentrated $TiCl_4$ was added dropwise into the prepared 8% PAN/DMF mixture and stirred in a fume hood until the white HCl fumes disappeared from the resultant sol gel. Moreover, 1.5 to 3 mL of 5% NH_4NO_3 was added dropwise into the C-TiO_2 sol gel obtained and stirred for 15 to 30 min until the color of the mixture slightly changed from brownish to yellow-brownish.

2.2. C-N-TiO_2 Film Procedure

The C-N-TiO_2 films on glass supports (substrates) were obtained through the spin coating method from a sol gel solution using a G3P-8 SPINCOAT (Specialty Coating Systems Inc., Indianapolis, IN, USA) as shown in Figure 1. Highly uniform films were achieved under the dynamic (spin drop) method compared to the non-uniform films obtained using the static (drop-spin) technique. Firstly, the glass supports (substrates) were cut into squares of 2 by 2 cm, cleaned thoroughly in acetone,

followed by isopropanol in an ultrasonic bath for 10 minutes, respectively, and thereafter repeatedly rinsed in deionized water and left to dry naturally.

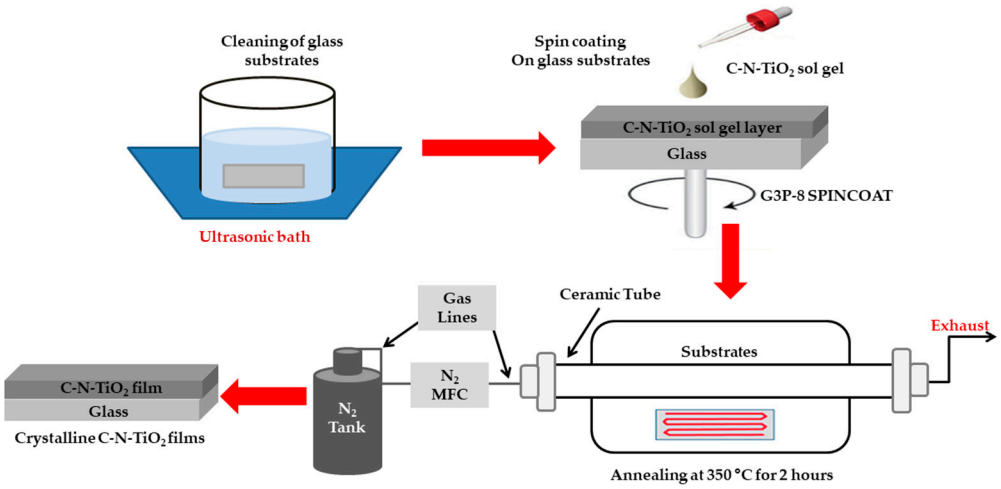

Figure 1. Schematic experimental set up used for spin coating of C-N-TiO_2 thin films.

The C-N-TiO_2 films were obtained using a spinning speed altered from 2000 to 2900 revolutions per minute (rpm) and the sol gel solution was varied by adding 3, 4, or 5 mL of gel per 5 mL of DMF solvent. A time of 90 s was used to allow the film to dry while spinning. Whitish films were visible immediately after spin coating confirming the successful and uniform deposition of sol gel films. These thin films were further annealed using a 3-zone horizontal ceramic-tube furnace (Brother XD-1600MT manufactured by Zhengzhou Brother Furnace Co., LTD, Zhengzhou, China) as described in Figure 1. The gel-coated glass samples were placed at the center of the heating zone, which achieved the desired temperature of 350 °C (ramping rate of 10 °C /min). The samples were left at this temperature for 2 h under a continuous flow of dry N_2 (Mass Flow Controllers (MFC)) to avoid any oxidation of the C-N-TiO_2 films formed while annealing. The system was cooled down under N_2 flow and the annealed C-N-TiO_2 films were dark in color.

The film C-N-TiO_2 thickness was measured using a profiler (Veeco DekTak 6M, stylus profiler, Veeco Instruments, Inc., Tucson, AZ, USA) with a low force of the stylus to avoid scratching of the films. The morphological distribution/deposition of the nano catalyst on the glass was investigated by scanning electron microscopy (SEM), while the composition of the coated films was investigated by energy dispersive spectroscopy (EDS). Furthermore, by changing both speed and sol gel to solvent volume ratio, the stability of the prepared films was assessed by the photocatalytic degradation of O.II sodium salt dye at the applied conditions.

2.3. Effect of Spin Coating Speed and Sol-Gel Dilution on the Thickness of Thin Films

The impact of spin coating rotation speed on the sol gel film thickness was investigated by varying the speed from 2000, 2300, 2600, to 2900 revolutions per minute (rpm) following the spin coating process described above, while the sol gel to solvent volume ratio (3:5) and the spinning time 90 s were kept constant. Conversely, the viscosity of the sol gel to solvent volume ratio (V:V) was examined by altering the gel volume from 3, 4, to 5 mL while that of DMF solvent (5 mL) was kept constant. So, three solutions ratios of 3:5, 4:5, and 5:5 were prepared and stirred for 24 h at room temperature and then also coated at a speed of 2600 rpm for 90 s following the same coating procedure shown in Figure 1. Each coating experiment and thickness measurement was performed twice (n = 2).

2.4. Application 1: Photo Catalysis Test

Furthermore, in both speed and sol gel to solvent volume ratio investigations, the activity of the C-N-TiO_2 films was assessed by the photocatalytic decoloration of O.II dye detailed in Figure 2

at the following conditions: O.II concentration 5 mg/L, volume 500 mL, solution pH 2.5, a UV lamp (Mega-Ray 160 W/240 V MR160 SPL11/14 from Kimix), the irradiation time of 120 min, and with sampling every 30 min. The absorbance of O. II dye was measured at a fixed wavelength of 485 nm and the unknown concentration of O.II solution was estimated using the linear trend $y = 0.0691x$ obtained from O.II dye standard solutions. The decoloration efficiency of O.II dye pollutant was estimated according to Equation (1).

$$\text{Decoloration}\% = \left(\frac{C_t - C_0}{C_0}\right) \times 100 \quad (1)$$

where C_0 represents the concentration of O.II dye at time $t = 0$ min and C_t the dye concentration at sampling time t.

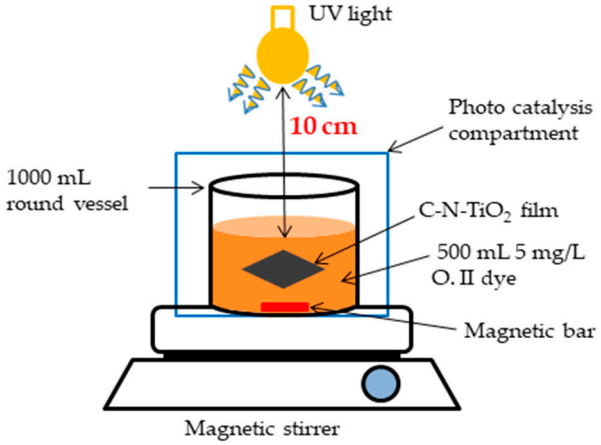

Figure 2. Photocatalytic experimental set up.

2.5. Perovskite Solar Cells Fabrication

The perovskite cell fabrication started with the cleaning process of patterned fluorine-doped tin oxide (FTO)-coated glasses (from PerkinElmer (UK) Holdings Ltd, Buckinghamshire, U.K.), firstly washed with a cleaning liquid, dissolved in deionized water. Subsequently, the glass supports were immersed in an ultrasonic bath with acetone and 2-propanol for 10 min for each step. The compact TiO_2 ($cTiO_2$) blocking layer (50 nm) was deposited by spray pyrolysis with a solution of acetylacetone (2 mL), titanium diisopropoxide (3 mL), and ethanol (45 mL) at 460 °C (all previous chemicals were purchased from Merck KGaA, Darmstadt, Germany). In the reference case, a thin mesoporous TiO_2 ($mTiO_2$) film (~150 nm) was deposited on top of the $cTiO_2$/FTO support by spin coating (3000 rpm for 20 s). The spun TiO_2 paste (Dyesol 30 NRD paste diluted in ethanol 1:5 in wt %) was sintered at 480 °C for 30 min in air. In the case of C-N-TiO_2-based devices, C-N-TiO_2 layers were realized according to the optimized procedure reported in Section 3.2.

A solvent mixture of anhydrous N,N-dimethylformamide (DMF), and dimethylsulfoxide (DMSO) in a 3:1 ratio (v:v) was used to prepare a $Cs_x(MA_{0.17}FA_{0.83})_{(1-x)}Pb\ (I_{0.83}Br_{0.17})_3$ triple cation precursor perovskite solution composed by a mixture of lead (II) iodide (PbI_2), lead (II) bromide ($PbBr_2$), methyl ammonium bromide (MABr), formamidinium iodide (FAI), and cesium iodide (CsI) (purchased from Greatcell Solar Materials Pty Ltd, Rome, Italy) by following the molar ratio suggested by Saliba et al. [27]. The obtained mixed perovskite solution was deposited with a one-step deposition and antisolvent method in a nitrogen-filled glovebox system by using a two-step program at 1000 and 5000 rpm for 10 and 30 s, respectively. During the second step, 150 µL of chlorobenzene was poured on the spinning substrate 7 s before the end of the program and the sample was immediately annealed at 100 °C for 1 h in a nitrogen-filled glovebox to obtain a compact perovskite layer 450 nm thick [28]. A 140-nm thick hole transport layer (HTL) was spin coated at 2000 rpm for 20 s using a Spiro-OMeTAD (73.5 mg in 1 mL of chlorobenzene) solution doped with 26.7 µL of TBP, 16.6 µL of Li-TFSI, and 7.2 µL Cobalt (III) FK209 complex [29] (all purchased from Merck KGaA, Darmstadt, Germany). Finally, a gold counter

electrode (~100 nm) was evaporated through a shadow mask on an active area of 0.1 cm^2 to complete the device.

2.6. Application 2: Perovskite Solar Cells

Devices testing: current density-voltage (*J*–*V*) characteristics of PSCs were measured under simulated AM 1.5 G solar light at 1000 W/m^2 irradiance generated by a solar simulator (ABET Sun 2000, class A, Abet Technologies, Inc. 168 Old Gate Lane Milford, Connecticut 06460) [30]. The system was calibrated with a certified reference Si Cell (RERA Solutions RR-1002 purchased from Rera Solutions B.V., Mercator 1 Building, Toernooiveld 200 6525 EC Nijmegen, Netherlands) and devices were measured using a mask to define the active area of 0.1 cm^2 [31].

3. Results

3.1. Effect of Spin Coating Speed on the Thickness of C-N-TiO_2 Thin Films

The influence of coating speed on the thickness of thin films of the sol gel precursor was assessed by using different spin speeds of 2000, 2300, 2600, and 2900 rpm while the sol gel-solvent volume ratio of 3 mL of sol gel diluted in 5 mL of DMF solvent (50 µL solution drop was used each spin coating) and spinning time of 90 s was kept constant. The thickness of films after thermal annealing at 350 °C was determined by Dektak profilometry analysis (n = 2) and the results of this investigation are presented in Table 1 and plotted in Figure 3. The results in Figure 3 show that the annealed C-N-TiO_2 film thickness correlated inversely with an increase in spin speed. The thickest films of 551 nm with 0.233 g of C-N-TiO_2 catalyst were achieved at 2000 rpm followed by 445 nm corresponding to 0.219 g of C-N-TiO_2 nano catalyst at 2300 rpm at the applied conditions described in Figure 3. Likewise, the coatings thicknesse of 356 and 243 nm with 0.219 and 0.217 g of C-N-TiO_2 nano composites were obtained at speeds of 2600 and 2900 rpm , respectively, as shown in Table 2. Consequently, the thinnest film corresponding to the lowest C-N-TiO_2 catalysts mass was achieved at a spin speed of 2900 rpm . These results showed that 243-nm thin films could be obtained at high rotational speeds, but the mass of the catalysts could be low. A similar trend related to the spin coating showed that the mass of the C-N-TiO_2 catalyst deposited on the glass decreased with an increase of spin coating speed. This further inferred that spin coating speed is a very crucial parameter in film engineering that needs to be considered. For optimization purposes in this study, 2600 rpm was selected as the optimum rotation coating speed that was used throughout the further tests. Even though various studies on immobilization of TiO_2 on glass were conducted [32–35]; only a few or no investigations studied the trend between sol gel spin coating speed and thickness of annealed film layers as described in this study.

Table 1. Effect of spin coating speed on the thickness of the C-N-TiO_2 films: sol gel: solvent ratio (*V*:*V*) = 3 mL of sol gel diluted in 5 mL of DMF solvent (3:5), spin coating time 90 s.

Coating Speed (rpm)	Sol gel to DMF Solvent Volume Ratio (*V*:*V*)	Annealed C-N-TiO_2 Film Thickness (nm) n = 1	Annealed C-N-TiO_2 Film Thickness (nm) n = 2	Average Thickness (nm)	Standard Deviation	Mass (g) of C-N-TiO_2 on Glass
2000	3:5	539.4	564.3	551.7	±17.4	0.2329
2300	3:5	459.6	432.1	445.9	±19.4	0.2198
2600	3:5	383.4	329.4	356.4	±38.2	0.2197
2900	3:5	329.1	157.1	243.1	±21.6	0.2169

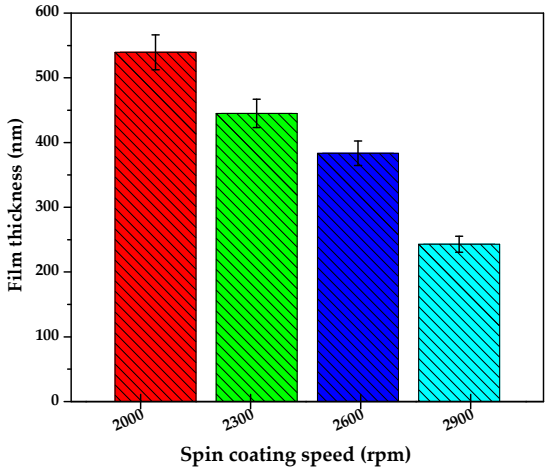

Figure 3. Effect of rotational coating speed on the annealed C-N-TiO_2 film thickness obtained at the following conditions: sol gel to solvent volume ratio (*V*:*V*) 3:5, spinning time 90 s. The samples were pyrolyzed in N_2 at 350 °C (ramping rate of 10 °C/min) for 105 min. The thickness measurements of each film were duplicated (n = 2).

Table 2. Mass (g) of C-N-TiO_2 deposited on films coated at different spinning speeds at the following conditions: sol gel-solvent volume ratio (*V*:*V*) 3:5, coating time 90 sec. The samples were thereafter pyrolyzed at 350 °C at a ramping rate of 10 °C /min for 105 min (n = 2).

Spinning Speed (rpm)	Average Mass of the C-N-TiO_2 Film (g)	Average Mass of the Uncoated Glass (g)	Mass of C-N-TiO_2 used (g)
2000	1.044	0.812	0.233
2300	1.031	0.812	0.219
2600	1.031	0.812	0.219
2900	1.028	0.812	0.217

3.2. Light Microscopy, Scanning Electron Microscopy, and Energy Dispersive Spectroscopy

The distribution of the sol gel precursor influenced the final annealed film of C-N-TiO_2 nano catalyst on the support and the presence of C, Ti, and O in the catalyst layers after the pyrolysis step was further evaluated by light microscopy (LM) and scanning electron microscopy coupled with energy dispersive spectroscopy (SEM-EDS) analysis, respectively. The LM images in Figure 4 obtained upon variation of speed show that coating layers present excellent structural integrity and improved adhesion on the glass support. The SEM images of the obtained C-N-TiO_2 films at each rotation speed are presented in Figure 5. The composition of each annealed film was measured by EDS and is presented in Table 3.

The SEM images present the morphologies of the annealed C-N-TiO_2 films that were prepared from the sol gel spun at rotational speeds from 2000, 2300, 2600, to 2900 rpm . Figures 4 and 5 show that the highly porous network of the C-N-TiO_2 nano catalyst was well dispersed on the glass surface after annealing in N_2 at 350 °C for 2 h. However, the morphology of the films changed with spin coating speed. For instance, unlike the uncoated glass (Figure 5a), Figure 5b,c showing glass coated at 2000 and 2300 rpm show that a distinctive needle-like morphology formed upon the glass support, testifying to a well dispersed nano-composite on the glass surface and the layer thickness was 339–564 nm and 432–459 nm, respectively. The SEM images of C-N-TiO_2 film coated at 2600 and 2900 rpm (Figure 5d,e) show C-N-TiO_2 was also well distributed on the support. Moreover, the SEM images of the films coated at 2900 rpm presented in Figure 5e clearly showed that thin layers (157 nm) of C-N-TiO_2 nano composite were not distinguishable from the support surface due to catalyst homogeneity on the support. The compact and condensed morphology in SEM images in Figure 5e suggested strong adherence between the nano-catalyst and the support. Nevertheless, the SEM results further proved

that the annealed nano catalyst adopted different morphologies on the support, depending upon coating at different rotation speeds.

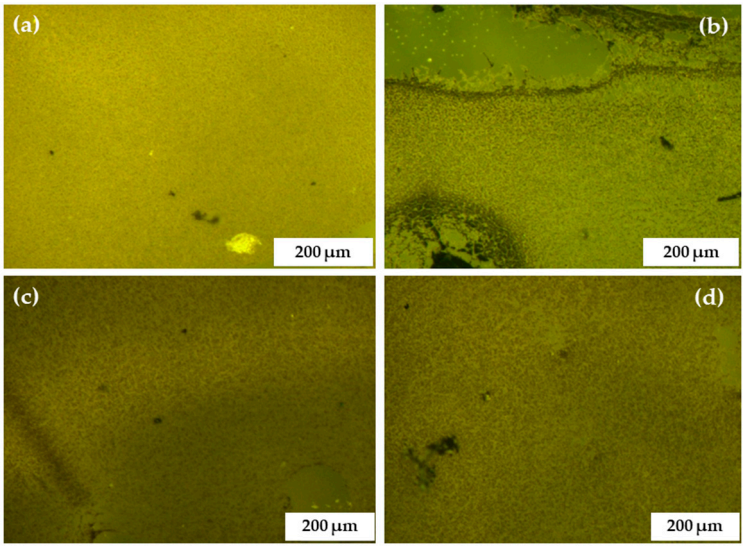

Figure 4. Light microscopic images of C-N-TiO_2 thin films recorded at calibration 90, at different speeds (2000 (**a**), 2300 (**b**), 2600 (**c**), to 2900 (**d**) rpm), and constant sol gel-solvent volume ratio of 3:5 for 90 sec. The samples were annealed in N_2 at 350 °C (ramping rate of 10 °C/min) for 105 min.

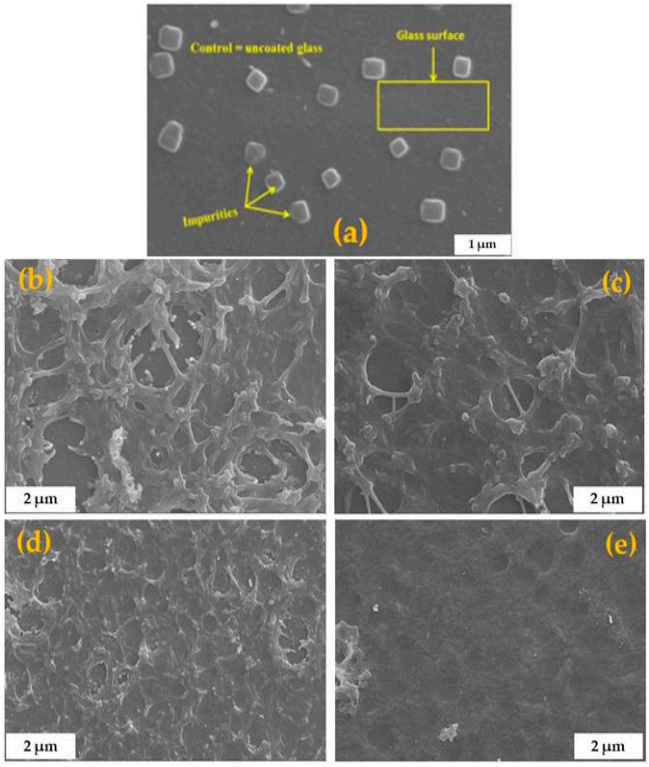

Figure 5. Scanning electron microscopy (SEM) morphology of uncoated glass (**a**) and annealed films of C-N-TiO_2 coated on support at different rotating speeds 2000 (**b**), 2300 (**c**), 2600 (**d**), to 2900 (**e**) rpm), and constant sol gel-solvent volume ratio of 3:5 for 90 s. The samples were annealed in N_2 at 350 °C (ramping rate of 10 °C/min) for 105 min.

The EDS results presented in Table 3 show that C, Ti, and O were present in the prepared thin films, and Ti content that decreased from 0.74 to 0.50 wt % could be tailored by spinning speed.

The high amount of C shows that PAN related C residues were present after annealing. However, N was not detected since its amount might have been lower than the detection limit/sensitivity of the EDS instrument. The results hence showed that regardless of the coating speed, nano C-N-TiO_2 film adhered to the glass support after the annealing process.

Table 3. Normalised weight percentages of elements C, Ti, and O in the films coated at different speeds and constant sol gel-solvent volume ratio (3:5) and coating time of 90 s, followed by annealing at 350 °C, at a ramping rate of 10 °C/min for 105 min.

Elemental Composition (w %) of Uncoated and C-N-TiO_2 Coated Films			
Samples	**C**	**O**	**Ti**
Uncoated glass	19.30	80.70	NA
Glass coated at 2000 rpm	21.34	77.92	0.74
Glass coated at 2300 rpm	19.45	79.83	0.72
Glass coated at 2600 rpm	21.12	78.38	0.50
Glass coated at 2900 rpm	20.62	78.86	0.52

3.3. Effect of Sol Gel–Solvent Ratio on the Thickness of Thin Films

The effect of sol gel viscosity on the thickness of the annealed film layers was assessed by varying the sol gel to DMF solvent volume ratio (v:v) from 3:5, 4:5, to 5:5, respectively, at a constant rotation speed of 2600 rpm for 90 s. The thickness of samples measured are presented in Table 4 and plotted in Figure 6.

Table 4. Effect of sol gel to solvent volume ratio (*V*:*V*) on the film thickness. Experimental conditions: spin coating speed 2600 rpm , spinning time 90 s, pyrolysis temperature 350 °C in N_2 (ramping rate of 10 °C/min) for 105 min (n = 2).

Sol Gel to DMF Solvent Ratio (*V*:*V*)	Coating Speed (rpm)	Film Thickness (nm) n =1	Film Thickness (nm) n = 2	Average Thickness (nm)	Standard Deviation	Film Mass (g) n = 1	Film Mass (g) n = 2	Average Mass (g) of the Film	Mass (g) of the Uncoated Glass	Mass of C-N-TiO_2 on Films
3:5	2600	356.4	359.8	358.1	±24.8	0.8579	0.8577	0.8578	0.8118	0.0460
4:5	2600	420.0	423.0	421.5	±21.2	0.8224	0.8222	0.8223	0.8118	0.0105
5:5	2600	453.0	456.6	454.8	±25.7	1.048	1.048	1.048	0.8118	0.2365

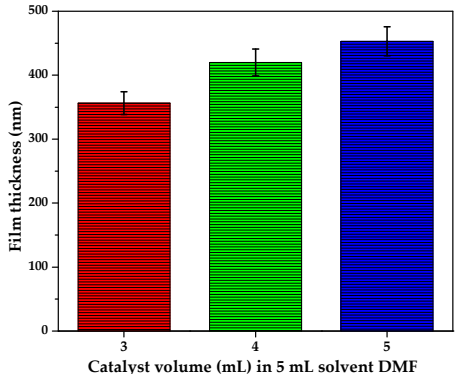

Figure 6. Effect of sol gel to solvent volume ratio on the thickness of films at the following conditions: coating speed 2600 rpm , spinning time 90 s, pyrolysis temperature 350 °C (ramping rate of 10 °C/min) for 105 min. The sol gel to solvent volume ratio (*V*: *V*) was varied from 3:5, 4:5, to 5:5. The thickness of each sample was measured twice (n =2).

The results show that the thickness of the films increased with an increase of sol gel to volume ratio. The thinnest catalytic layers (358 nm) corresponding to 0.0460 g of C-N-TiO_2 nano catalyst were obtained at sol gel to solvent ratio of 3:5 while the thickest film layers 420 nm and 453 nm with 0.0105 and 0.2365 g of C-N-TiO_2 nano composites were achieved at 4:5 and 5:5 sol gel to solvent

volume ratio, respectively. This implied that the ratio of 3:5 was the most suitable for the spin coating performed in this study. Likewise, the less diluted 5:5 sol gel-solvent ratio was more viscous and might have evaporated less during the spin coating and annealing process, resulting in a film with a higher mass of 1.048 g. This in turn resulted in thicker layers similar to those reported by Lu et al. [36], Kenanakis et al. [37], Zabihi et al. [38], and Clausi et al. [39]. Based on these results and for optimization purposes, 3:5 was identified as the optimum sol gel-solvent ratio in this study.

3.4. Light Microscopy, Scanning Electron Microscopy, and Energy Dispersive Spectroscopy

The effect of sol gel to the solvent ratio on the thin film morphology was examined by various characterization techniques, among which, light microscopy (LM) and scanning electron microscopy (SEM) paired with energy dispersive spectroscopy (EDS) [38]. In this study, LM (Figure 7) and SEM (Figure 8) were used to visualize the deposition/distribution of the nano composites on the supports. The energy dispersive spectroscopy (EDS) in Table 5 coupled to SEM was used to prove the presence of C, Ti, and O though N could not be identified due to the low sensitivity of the SEM instrument toward its amount in the catalyst. The LM and SEM images of films fabricated at each sol gel-solvent ratio (3:5, 4:5, and 5:5), are presented in Figures 7 and 8.

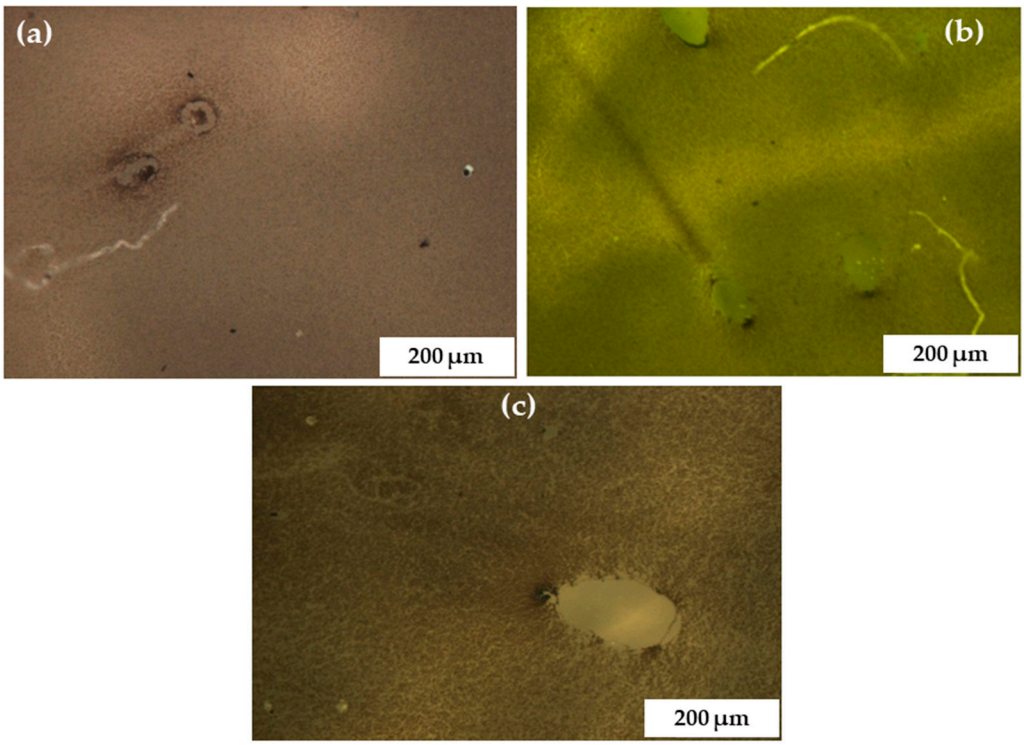

Figure 7. Light microscopic images recorded at calibration 90 of C-N-TiO_2 coated on glass support at a sol gel-solvent ratio varied from 3:5 (**a**), 4:5 (**b**), to 5:5 (**c**), and constant spinning speed of 2600 rpm for 90 s followed by pyrolysis at 350 °C in N_2 (ramping rate of 10 °C /min) for 105 min.

The SEM images show that the annealed C-N-TiO_2 coatings were well distributed on the glass surface. Despite increasing the sol gel-solvent ratio, the nano catalyst was well dispersed on the substrate (Figure 7). In Figure 8a, C-N-TiO_2 was well fused on the glass, hence resulting in porous films with a thickness of 358 nm as previously described in Table 4. The fusion of C-N-TiO_2 upon the glass surface suggested that there was a strong adherence or bonding between the nano catalyst and support at a low sol gel to solvent ratio. The low viscosity of the precursor sol gel to solvent in a ratio of 3:5 led to thin layer films, which were fused to the support when spin coating at an optimized rotation speed of 3600 rpm followed by thermal annealing. In contrast, SEM images in Figure 8b,c show that a porous C-N-TiO_2 network was produced at viscosities of 4:5 and 5:5 on the support surface. Consequently,

the elevated sol gel content led to nanocrystalline structured films with thicknesses of 420 to 453 nm when spin coated at a specific rotation speed of 2600 rpm and subsequently thermally annealed. Table 5 confirms that C, Ti, and O were present in C-N-TiO_2 immobilized on the glass. Ti content showing a light increase from 0.50, 0.52, to 0.78 wt % could be controlled by altering the viscosity of the sol gel. Whereby, the elevated amount of carbon was probably due to C residues resulting from the annealing process from the decomposition of PAN.

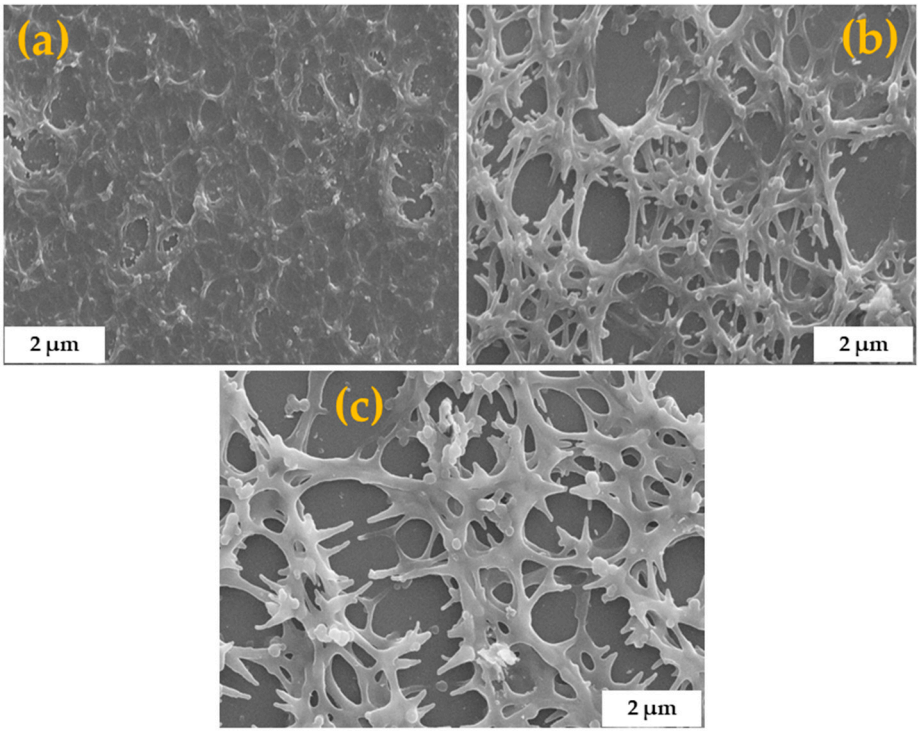

Figure 8. SEM morphologies of C-N-TiO_2 coated on support at a sol gel-solvent ratio varied from 3:5 (**a**), 4:5 (**b**), to 5:5 (**c**), and constant spinning speed of 2600 rpm for 90 s followed by pyrolysis at 350 °C in N_2 (ramping rate of 10 °C /min) for 105 min.

Table 5. Weight percentages of elements C, Ti, and O in the films coated at different sol gel-solvent ratio (*V*:*V*) at a constant speed (2600 rpm) and coating time of 90 s followed by annealing at 350 °C, at a ramping rate of 10 °C /min for 105 min. Elemental composition (wt %) of uncoated and C-N-TiO_2-coated films.

Sol gel to Solvent Ratio (*V*:*V*)	C	O	Ti
Uncoated glass	19.13	80.87	NA
3:5	21.12	78.38	0.50
4:5	22.96	76.52	0.52
5:5	22.87	76.33	0.78

3.5. Application 1: Photo Catalysis Tests

3.5.1. Effect of Spin Coating Speed on the Degradation of Orange II Sodium Salt Dye

The photocatalytic activity of the prepared thin films was evaluated by the degradation of O.II sodium salt dye at the applied conditions. Beforehand, O.II was exposed to UV light for 120 min and was considered as control (UV alone). The photo catalysis results showed that decoloration% of orange II with UV light alone slightly increased up to 4.8% with an increase in treatment time. This might be because the azo group (–N=N–) was progressively being destroyed as UV-vis light exposure time gradually increased. The results of the duplicated activity are shown in Figure 9.

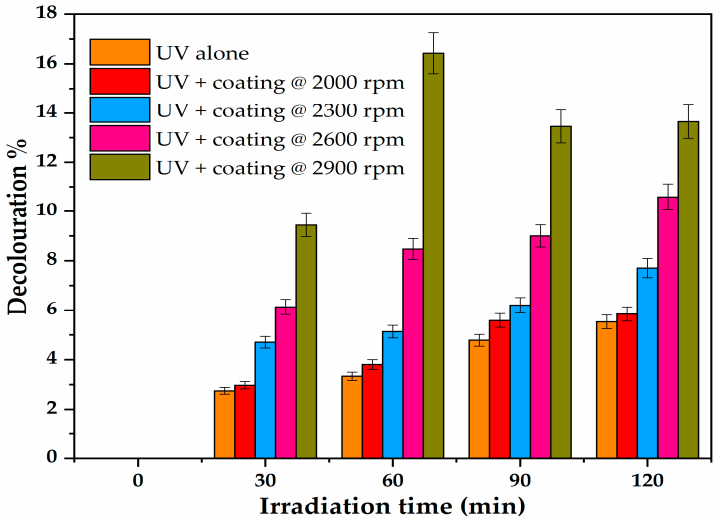

Figure 9. Photocatalytic activity of glass coated with C-N-TiO_2 nano composites at spin coating speed that varied from 2300, 2600, to 2900 rpm at the following experimental conditions: [O.II] concentration 5 mg/L, volume 500 mL, of pH 2.5, and sampled at 30 min intervals over an irradiation time of 120 min. Each photo catalysis experiment was duplicated (n = 2).

The UV-Vis photo catalysis outcomes show that O.II decoloration% increased with exposure of the dye to composite coatings that were prepared using an increase of spin coating speed up to 2600 rpm . The photocatalytic activity films made at 2900 rpm were most consistent over time. The highest decoloration percentage of O.II was obtained with thin layers of C-N-TiO_2. After 60 minutes of UV-Vis exposure, about 16.43 and 9.23% removal of O.II were obtained with films coated at 2600 and 2900 rpm , respectively, followed by 5.12, 3.80, and 3.33% of O.II removal achieved with films coated at 2300 and 2000 rpm and UV alone, correspondingly. This low activity could be ascribed to the small sample size relative to solution volume and dye concentration and further to the decrease of Ti content (from 0.74 to 0.52 wt %) dictated by EDS shown in Table 3. Alternatively, the photocatalytic outcomes in Figure 9 inferred that thicker layers resisted light penetration, which in turn induced low degradation of O. II. The results also show the film stability in acidic conditions.

Indeed, during photo catalysis with thick layers, most electrons and holes might have been created in the bulk of the doped nano semiconductor, and hence could not reach the surface of the film where the photocatalytic reaction took place. This consequently resulted in the lower photocatalytic degradation of O.II [14]. This trend for the thicker films was also observed after 30, 90, and 120 min of UV irradiation. In the case of films coated at 2600 rpm , the 15.3% O.II removal obtained after 60 minutes decreased to 12.67 and 12.83% after 90 and 120 min of treatment. This suggests that the films coated at 2600 rpm maximally absorbed the UV light after 60 minutes of UV irradiation.

Beyond this time, the thin layer of 353 nm films became less active in O.II acidic medium. The current study shows that the highest photocatalytic degradation percentages of O.II were achieved at lower film thicknesses. In other words, the degradation of O.II increased with a decrease in film thickness to about 350–250 nm. It can be inferred that high photocatalytic activities of composite films can be achieved with films of thickness ≤300 nm as the thinnest films obtained in this study fit within this range. Hence it could be inferred that the photocatalytic activity of sol-gel spin coated films is significant in a thickness range of ≤300 nm relative to the rotational spin coating speed. Conclusively, the thickness of the TiO_2 films has an impact on their Ti content and thus their photocatalytic activities and should therefore be controlled to reach the desired activity.

The results obtained in this study demonstrated that during the preparation of thin films by the spin coating process, the rotational speed is an important parameter that may influence the morphology of the films and their Ti content per unit area, which further impacted their photocatalytic activity.

Hence spin coating speed should be optimized to achieve the desired Ti content through controlling the layer thickness and so improve photo catalytic performance of the prepared films.

3.5.2. Effect of Sol Gel to Solvent Ratio on the Photocatalytic Activity of Coated Glass on Orange II Dye Removal

The photocatalytic test of the films fabricated using sol gel at different viscosities followed by annealing on their removal of O.II sodium salt dye at the applied conditions is plotted in Figure 10.

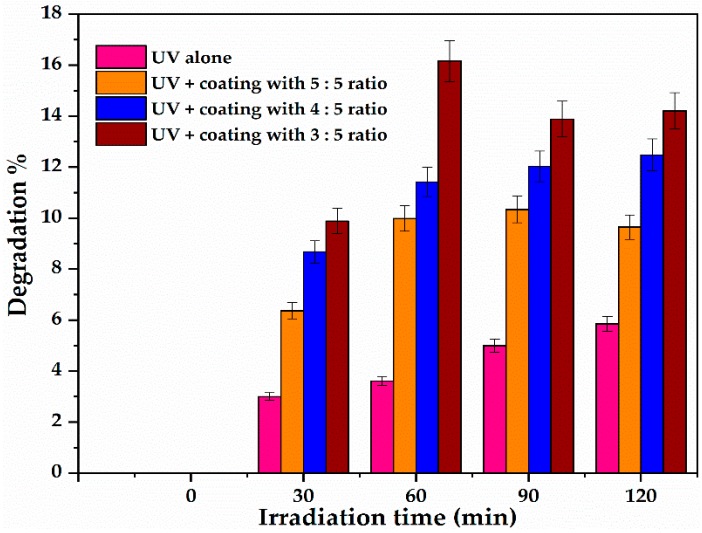

Figure 10. Photocatalytic activity of glass supported C-N-TiO_2 coatings formed at sol gel-solvent ratio from 3:5, 4:5, or 5:5 (Experimental conditions: O.II concentration 5 mg/L, volume 500 mL, pH 2.5, and irradiation time of 120 min. The experiment at each sol-gel to solvent ratio was duplicated (n = 2).

At each sampling time, the results in Figure 10 show that O.II decoloration correlated inversely to the sol gel to the solvent ratio used during film preparation and following the increase of Ti content that rose from 0.50 to 0.78 wt % as shown in Table 5. After 30 minutes of UV-Vis irradiation, 5.3% of degradation was obtained with the 5:5 ratio. This implied that the films with thick layers resulting from high viscosity had lower decoloration% of O. II. The highest (15.42%) O.II decoloration was reached after 60 minutes of UV-Vis exposure at a 3:5 sol gel to the solvent ratio. This then decreased to 12.67 and 12.83%, and hence became constant [40–42]. This indicated that at 60 minutes of reaction time, the supports coated with 3:5 sol gel to solvent ratio reached maximum UV-light absorption and the samples were stable in O.II acidic medium. Conversely, this shows that films with low thicknesses achieved at low sol gel to solvent ratio were more photocatalytically active than thicker ones and consequently led to improved decoloration% of O.II dye [37,43–45]. It should be recalled that the concentration of gel/dopants and the viscosity of the gel are directly linked to one another. That is the more sol gel to the solvent used, the more viscous the sol gel. Therefore, spin coating small amounts or a low concentration of the gel on the substrates resulted in improved morphological properties of the prepared films. In this regard, films coated with low viscosity resulted in thin films of desired thickness and therefore improved Ti content and photocatalytic activity.

These results meant that the films with thicker layers in the range of 420–453 nm resisted UV-light penetration in an aqueous acidic environment, which also could be due to the C-N-TiO_2 photo catalyst being occluded in the carbon matrix used to adhere the catalyst to support. Alternatively, the excited electrons in the coated films did not reach the film surface where the reaction occurred and rather accelerated the electron-hole recombination process resulting in reduced photocatalytic activity of the prepared nano films. This conforms with the findings of Dijkstra et al. [42] and Varshney et al. [44], who highlighted that one of the few disadvantages of the sol-gel spin coating process is the fact that it is often difficult for thick layers of films to be active when exposed to photo oxidative environments.

This study proved that spin coating under optimized conditions is an adequate technique that can be used to immobilize active catalysts on flat supports. However, the speed of spin coating and catalyst to sol gel ratio are two parameters among various that need to be cautiously tuned to obtain thin films of the desired thicknesses and activity [46].

The steadily increasing photocatalytic decoloration% of O.II obtained here (below 20% overall) was mainly due to the small sample size relative to the volume and concentration of dye used. This on the other hand demonstrated that the engineered films resist delamination when exposed to harsh oxidative environments. This method can therefore be used to avoid post-separation/filtration of aqueous powder photo catalyst that is often a pertinent limitation in photo catalysis at an industrial scale.

3.6. Application 2: Perovskite Solar Cells

Replacement of $mTiO_2$ by C-N-TiO_2

Usually, mesoscopic n-i-p perovskite solar cells (PSCs) require very high temperatures (above 480 °C) to sinter the m-TiO_2 layer after the deposition. While for small devices, the sintering step does not impact on device production, in the case of large area modules [47,48], it can cause support deformation and/or bending that then negatively affect the following module production steps, such as laser ablations [48], in terms of substrate alignment and reproducibility. Since the as-optimized C-N-TiO_2 was annealed at a moderate temperature of 350 °C, it was further tested as an electron transporting layer in perovskite solar cells employing n-i-p structure. The thin films on the support were engineered by spinning 50 µL of diluted sol gel with DMF solvent at different ratios of 3:5, 4:5, and 5:5 and rotational of speed 2600 rpm for 90 s. All samples coated at these conditions were annealed at 350 °C (ramping rate of 10 °C/min) for 2 h under dry N_2 gas.

Alternatively, reference cells were fabricated by using TiO_2 paste-based solution (30 NRD diluted in ethanol 1:5 *w*/*w*) as mesoporous layer precursor, spun at 3000 rpm for 20 s on top of the cTiO_2 layer, and finally sintered at 480 °C for 30 seconds to remove completely the organic binder present within the paste [49]. The detailed procedure for realizing complete perovskite devices is reported in the Materials and Methods section. The typical current density–voltage characteristics for both the best performing reference (standard m-TiO_2) and C-N-TiO_2-based devices recorded under 1 SUN (1000 W/m^2) irradiation are reported in Figure 11 and the key photovoltaic (PV) median parameters including power conversion efficiency (PCE), short-circuit current density (J_{sc}), open circuit voltage (V_{oc}), and fill factor (FF) coupled to their standard deviation of both devices are shown in Table 6. As a first observation, we demonstrated the use of C-N-TiO_2 as an electron transporting layer in perovskite solar cells by recording decent averaged power conversion efficiency overcoming 9% (see Figure 11).

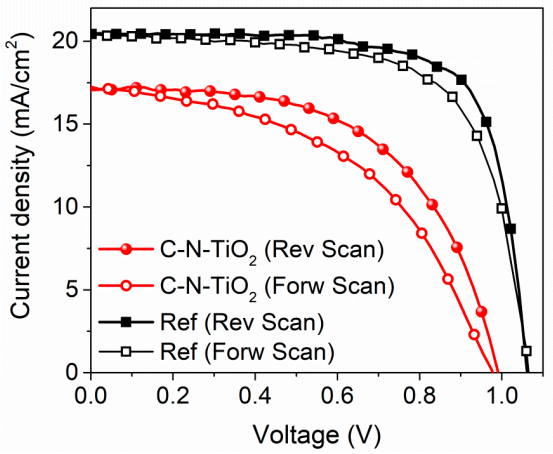

Figure 11. Current density–voltage characteristics for both the best performing reference (standard $mTiO_2$) and C-N-TiO_2-based devices under 1SUN (1000 W/m^2) irradiation in forward and reverse scan directions.

Table 6. Averaged (Av.) electrical parameter values and standard deviation calculated over six devices.

Samples	Av V_{OC} (V)	Av J_{SC} (mA/cm^2)	Av. FF (%)	Av. PCE (%)
Reference	1.06 ± 0.02	19.42 ± 0.86	73.14 ± 1.76	14.98 ± 0.71
C-N-TiO_2	0.99 ± 0.02	16.99 ± 0.44	54.79 ± 2.98	9.28 ± 0.52

The photovoltaic Figures of Merit (FoM) obtained for the two device typologies under one - sun (1 SUN) irradiation are reported in Figure 12. Despite the C-N-TiO_2-based cells exhibiting lower device performances when compared to reference devices, there is still room for improvement by looking at the obtained FoM. In particular, PCE of C-N-TiO_2-based cells can be improved by optimizing the uniformity and the thickness of the C-N-TiO_2 layer, since it can penalize both the perovskite layer morphology and the TiO_2/perovskite interface by eventually penalizing the absorbance of the perovskite layer and the electron transfer from perovskite to the electron transport layer (ETL), respectively, which can easily explain the overall short-circuit current density (J_{SC}) drop. Consequently, the unbalanced hole and electron extraction occurred by negatively affecting the device fill factor (FF).

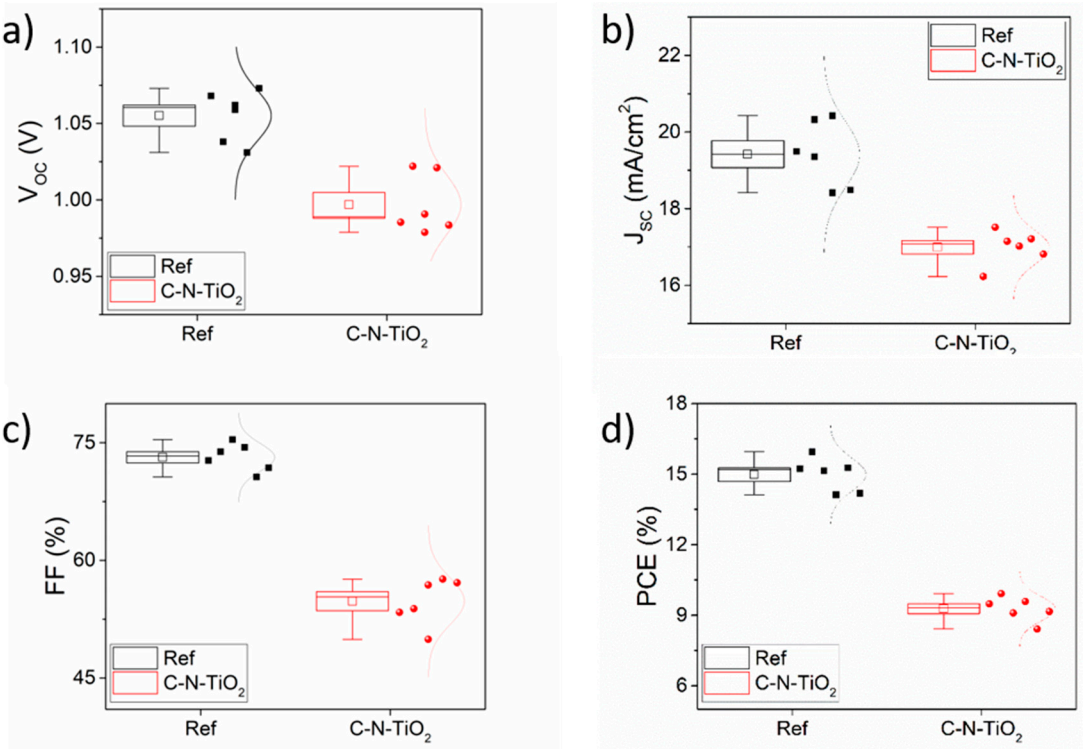

Figure 12. Photovoltaic Figures of Merit (FoM) of reference perovskite solar cells (PSCs) and C-N-TiO_2-based devices extracted from the current-voltage (*I-V*) characteristics measured under one-sun (1 SUN) illumination: (**a**) open-circuit voltage (V_{OC}); (**b**) short-circuit current density (J_{SC}); (**c**) fill factor (FF); and (**d**) power conversion efficiency (PCE). The relative standard error reported as error bar is extracted by measuring six devices.

Moreover, the observed reduction of open circuit voltage (V_{OC}) can be imputed to a not-perfect energy level alignment at the perovskite/C-N-TiO_2 interface. Surface treatments [50], the insertion of a proper 2D material interlayers [51,52] in terms of interface engineering and/or material work function tuning by Agresti et al. [53], could help achieve such energy level matching [54].

4. Discussion

Various authors endorsed that the immobilization of a catalyst on transparent supports such as glass using spin and spread coating was identified as an alternative cost-effective route for catalyst

coating [55,56]. That is, a controllable affinity between catalyst and glass supports was observed even though the limitations of catalysts coated on the glass are still under investigation [24,57]. Nevertheless, the effect of common factors mainly the rotation speed, the sol-gel to solvent volume ratio, and the evaporation rate to some extent on the thickness of the fabricated films and TiO_2 content are still being investigated [58,59]. In the current study, the effect of two key parameters including spin speed and catalyst to solvent volume ratio on the thickness and activity of the C-N-TiO_2 nano catalyst-coated films were examined. The outcomes in Figure 3 showing the decrease of film thickness with an increase of spin speed prove that coating speed is a crucial parameter in spin coating protocol that may further impact the photo catalysis of the films. The decrease of film thickness from 551 nm to 243 nm indicated that the solution evaporated more at higher speeds due to the centrifugal forces that force the sol gel in the outward direction of the support [60]. Considering the 2000–2900 rpm spin speed range used in our study, the best thickness 241 nm achieved at 2900 rpm shows that controlling rotational speed and sol gel evaporation followed by controlled annealing can lead to the formation of thin monolayer TiO_2 films with excellent smoothness as confirmed by light microscopy images shown in Figures 4 and 7.

Similar studies involving the impact of spin speed on various factors during sol-gel spin coating were highlighted. For instance, Khanna et al. [60] designed a long-range ordered close-packed monolayer of silica nanospheres with a size of approximately 200 nm deposited on silicon substrate by three-step spin coating method at ambient conditions. During their research, the influence of spin speed (varied from 200, 500, 1500 rpm) on the surface coverage of the film was investigated. The outcomes of their study showed that the film coverage thickness decreased with an increase of spin speed; however, various forces including centrifugal, capillary forces, solvent evaporation, and immersion capillary force were found responsible for the dispersion of the solution toward the outer edge of the film. The authors further confirmed that uniform domains on films were achieved at a spin speed of 200, 500, and 1500 rpm with an estimated surface covering ranging between 85–90% and comparable with results achieved by Wang et al. [61].

The extended effect of spin speed on the transmittance was inspected by Wang et al. [62] during the synthesis of uniform silver nanowires from AgCl seeds for transparent conductive films (TCFs) at spin-speed varying from 200, 500 to 1000 rpm . The finding of their study showed that the corresponding transmittance of the PET films engineered at the speed were 92, 81, and 95%, correspondingly. Likewise, Wang and co-authors, [62] endorsed that though optimisation of this parameter is crucial in spin coating process, it would be advantageous to engineer high-performing films at different speeds than fixed values to achieve desired catalyst layers.

Indeed, at higher revolutions per minute (rpm) speed, the catalyst being deposited was quickly spread/distributed on the surface of glass support leading to thinner films. Likewise, the catalyst layer may poorly or strongly adhere to the support depending on the chemical coordination/bonding behavior between the catalyst and support. This follows Chen and Dionysiou, [58] who highlighted that the desired properties of the obtained thin films have often good adherence with the catalyst to the support, thickness, porosity, and the durability of the catalyst or the catalyst lifetime. The poorly coordinated catalysts could be washed away when exposed to harsh oxidative environments while the intensely bonded catalyst could resist oxidative attacks and remain durable on the glass substrate.

The SEM morphologies presented in Figure 5 support the thickness data shown in Table 1 and Figure 3. The images displayed in Figure 2 indicate that the porous C-N-TiO_2 nano composites were successfully spread on glass support; however, its layer thickness progressively decreased until it became indistinguishable from the glass support as spin rotational speed was raised to 2900 rpm . Similar observations were previously highlighted by Guillard et al. [40] and Gültekin et al. [63], even though different catalysts and experimental conditions were used in their studies. The EDS results in Table 3 also show a slight fluctuating decrease of C and Ti content as spin speed was increased to 2900 rpm.

The coordination behavior between catalyst and support may also depend on the catalyst viscosity; in this regard, low viscosity could accelerate its evaporation during the sol-gel spin coating scenario [64].

Therefore, the findings in Table 4 and Figure 6 reinforce that the catalyst to solvent volume ratio influences the thickness of the film. The increase of C-N-TiO_2 catalyst thickness from 358 to 421 and 454 nm observed when sol gel to solvent volume ratio was altered from 3:5, 4:5, to 5:5 also showed that the best thickness was achieved at lower sol gel to solvent ratio, and hence implied that this parameter should also be taken into account during the sol-gel spin coating process. The EDS results in Table 5 also sustained the trend highlighted above where Ti content slightly increased with an increase of catalyst to solvent ratio. This was further complemented by SEM morphologies in Figure 8 showing fused catalyst with glass support in Figure 8a at low catalyst to solvent ratio 3:4. From the outcomes of our study, it can be inferred that besides various instructive results on sol-gel spin coating previously reported [65–67], spin speed and catalyst to solvent ratio can also significantly affect TiO_2 content and the film thickness, and hence their optimization is mandatory to achieve adequate and durable film layers.

The change in film thickness discussed above also impacted on the catalytic activity of the films. Thus, the photocatalytic outcomes in Figures 9 and 10 strongly show that moderately elevated percentages up to 17% of O.II dye removal were achieved with thinner films during both alteration of the spin speed and sol gel to solvent volume ratio. These minimal percentages could be due to the small mass values (0.233, 219, 219, 217 g) recorded in Table 2 and (0.0460, 0.0105, 0.2365 g) in Table 4 of the C-N-TiO_2 nano catalysts on glass that were immersed in large volumes 500 mL of 5 mg/L O.II simulated dye. The impact of solution volume and concentration on such small 2 × 2 cm films will be part of our future investigation. Our findings clearly show the correlation of mechanical properties and film thickness to photocatalytic performance of thick and thin C-N-TiO_2 films decorated on glass supports.

Indeed, during the annealing of C-N-TiO_2 films, foreign elements from the surface of the film might have diffused into the glass support leading to thin layers, and hence the rapid circulation of electrons that enhanced photocatalytic activity under UV irradiation. On the contrary, in thicker films, the excited electrons did not reach the film surface during UV illumination where the reaction occurred and probably accelerated the electron-hole recombination process [14]. This consequently resulted in reduced photocatalytic activity of the prepared nano films.

The film thickness-related photocatalytic activities were assessed by Danish et al. [41] upon the degradation of the methylene blue (MB) dye observed. The outcomes of their study showed that the removal percentage of MB decreased with a decrease in film thickness.

Consequently, the highest MB degradation percentage (95%) was achieved with 160.3-nm film while the lowest MB removal percentage 73% was reached with 112.8-nm thin films. This was also supported by Guillard et al. [40], Varshney et al. [44], and Arabatzis et al. [45], who reported that high photocatalytic activity could be reached with films of low surface roughness. This was further reinforced by various authors [43,68,69]. Our pollutant removal efficiencies seem less than those previously reported probably because the 2 × 2-cm C-N-TiO_2 films were immersed in a huge solution volume pf 500 mL of 5 mg/L O.II that impeded the penetration and minimized the focus of UV light adequate to induce effective photocatalysis process on the coated faces of films. This in return reduced the degradation percentages of O.II dye.

The effect of spin speed on photocatalytic activity thin films has extensively been reported in the literature, though different results were obtained [55,56]. Extensive investigations on the sol-gel spin coating of doped TiO_2 films on glass were reported [24,57]. The impact of viscosity on the photocatalytic activity of the films was also highlighted by Zabihi et al. [38] and Pérez et al. [69]. This was previously appealed by Hassan et al., [70] who stated that the presence of C or N in the TiO_2 lattice controls the photocatalytic sites and hence the photocatalytic activity. Altogether, these results further sustain that at an optimized sol gel to solvent ratio, with support cleaned with a suitable solvent system; it is possible to engineer thin films of desired thicknesses [46].

Unlike most photocatalytic studies discussed above that were performed in visible light, the photo catalysis test of the prepared C-N-TiO_2 films in our study was conducted under UV light to overcome limitations of using powder catalysts in our dielectric barrier discharge (DBD) reactor technology

previously studied [71]. Hence coating C-N-TiO_2 on glass could promote the efficiency of UV light generated in advanced oxidation processes to achieve maximum degradation of targeted water/air pollutants. Alternatively, one of our future tasks will be to investigate the efficiency of C-N-TiO_2-coated films under solar light as the thin and thick films developed in this study are favorable potential photo catalysts and perhaps suitable charge transport layers for photovoltaic applications.

The engineering of nanomaterials effective for both photo catalysis and photovoltaic applications is one of the challenging tasks in material science; nevertheless, various attempts were made in recent years [72–74]. Despite the photocatalysis scenarios and their benefits previously discussed, solar cell technologies are considered as outstanding prospects for renewable energy harvesting. Indeed, the efficiency of a solar cell is determined by measuring the amount of current density following applied voltage during light irradiation. Dubey et al. [75] conveyed that the main characteristic for a particular solar cell includes the short-circuit current density (*Jsc*), the open circuit voltage (*Voc*), and the fill factor (*FF*), which were explored in our study and the trends observed are presented in Figures 11 and 12.

The fill factor (*FF*) often expressed as $FF = Pmax/Jsc \times Voc$ is the squareness of the curve depends on the parametric resistance in solar cell machinery. Figures 11 and 12 represent the solar efficiencies of a perovskite cell developed in our study, showing the charge carrier layers were decorated with mTiO_2 and the sol gel-synthesized C-N-TiO_2 nanocomposites. The solar efficiency of the C-N-TiO_2 cell reached 9% and is lower than 15% obtained with the reference mTiO_2. Even though it was expected that C-N-TiO_2 would efficiently improve energy harvesting as compared to the base, various factors including electronic, optical, and mostly poor homogeneity might have decelerated the C-N-TiO_2-coated solar cell efficiency. Indeed, the SEM analysis in Figures 5 and 8 depicting the morphology of C-N-TiO_2 show irregular mesoporous microdomains of C-N-TiO_2 nano catalysts on films when both parameter spin speed and catalyst to solvent volume ratio were varied. These random porous holes were certainly due to strong centrifugal, solvent evaporation, and immersion capillary forces that unevenly dispersed the sol gel toward the edge of the support [76]. Parallel outcomes showing agglomerated and irregular shapes of nanocrystalline alumina particles prepared by the sol-gel method were also reported by Wannaborworn et al. [76]. The SEM images in Figures 5 and 8, therefore, taught us it would be advantageous to spin coat thin films at different speeds and catalyst to solvent volume ratios, as these two parameters are crucial and require adequate optimization.

The discontinuous homogeneity of C-N-TiO_2 films observed in Figures 5 and 8 might have induced short circuits during the solar cell energy conversion test, consequently resulting in low efficiency of 9% of C-N-TiO_2 compared to the reference. In comparison with the literature, the performance of C-N-TiO_2 solar cell with 9% conversion efficiency was much higher than the values reported in previous investigations [77–79]. Besides, Dong et al. [80] used hydrothermal protocol to synthesize TiO_2 and Ag-doped TiO_2 (Ag-TiO_2) nanoparticles that were used in the dye-sensitized solar cell (DSSC) application. Their outcomes showed that 6.44 and 5.05% solar conversion efficiencies were achieved with TiO_2 and Ag-TiO_2 nanoparticle-based dye-sensitized solar cells (DSSC), respectively. Their findings were hence lower than the 9% obtained in Figure 11. Comparable studies showing solar energy conversion efficiencies lower than that reported in Figure 11 were reported [81,82]. Nevertheless, this is the first time sol gel-synthesized C-N-TiO_2 has been employed in a photovoltaic application and we positively believe that succinct optimization of sol gel chemical composition as well as electrical parameters in the fabricated perovskite solar cell, the choice of appropriate film support, and perhaps following synthetic procedures suggested by Dubey et al. [75], Wu et al. [83], and Junfang et al. [84] could improve C-N-TiO_2 solar energy conversion efficacy.

5. Conclusions

In this study, a C-N-TiO_2 nano catalyst prepared by a sol gel method was successfully immobilized on glass support by the spin coating technique followed by annealing in N_2. We found that the spinning rotation speed and sol gel to solvent ratio significantly affected the thickness of the films

and Ti content, which further impacted on their photocatalytic performance. The distribution of C-N-TiO_2 nano catalysts on glass support after thermal annealing as seen by SEM analysis showed strong bonding adhesion between the nano composite and the support. The thinnest films showed higher photocatalytic activity compared to thicker ones. The overall percentage removal of O.II over time suggested that the prepared films were stable in O.II acidic milieu and oxidative conditions of free radicals.

Thus, proper optimization of spin coating parameters is essential to achieve the desired properties of the nanostructured films. Furthermore, we demonstrated that C-N-TiO_2 can be used as an electron transporting layer in perovskite solar cells by achieving not yet optimized but repeatable power conversion efficiencies above nine percent. In this regard, the lowering of TiO_2 ETL annealing temperature can help prevent the typical glass deformation experienced by employing sintering temperatures over 450 °C, which can negatively impact large device production such as modules or panels.

6. Novelty

Our study revealed for the first time that C-N-TiO_2 films are photo catalytically active, resistant in harsh environments, and are adequate charge carrier layers efficient enough for energy harvesting in solar cell technologies.

The sol gel C-N-TiO_2 nano catalyst spin coated on glass supports were active in both degradation of persistent organic O.II dye and solar energy conversion in perovskite cells. This study, therefore, showed that for a typically advanced oxidation dielectric barrier system generating UV light, the C-N-TiO_2 nano catalyst can directly be spin coated on the glass to enhance the efficacy of generated UV light. We further demonstrated that C-N-TiO_2 films can be used as an electron transporting layer in perovskite solar cells by achieving repeatable power conversion efficiencies above nine percent. These outcomes have not been outlined elsewhere. Here, we evidenced that the immobilisation of C-N-TiO_2 sol gel by spin coating technique resulted in thick and thin films profitable for both photo catalysis in advanced oxidation processes and photovoltaic applications.

Author Contributions: E.S.M.M., S.N., S.P., A.D.C., A.A., C.J.A. and L.F.P. planned the research and prepared the nano catalyst films, M.D., A.V., A.C.P., M.B., L.F.P., S.N., C.J.A., and E.S.M.M. performed the characterisation of the C-N-TiO_2 nano films and tested their activity upon decolouration of O.II dye under UV irradiations and their efficiency in Perovskite Solar Cells. E.S.M.M., L.F.P., S.P., A.D.C., A.A., M.D., M.B., S.N., C.J.A., examined the data and provided positive input in data interpretation and supervised the work. E.S.M.M., L.F.P., S.N., C.J.A., and A.A. wrote the first draft of the manuscript. All authors have read and agreed to the published version of the manuscript.

Funding: The authors are thankful for the financial support from NRF South Africa. M.D., A.V., A.C.P., and M.B. are grateful for the support of the Romanian Ministry of Research and Innovation through the Core Program, Project No. 18N/2019.

Acknowledgments: We thank NRF South Africa for the financial support of this Project. M.D., A.V., A.C.P., and M.B. acknowledge the support of the Romanian Ministry of Research and Innovation through the Core Program, Project No. 18N/2019, the infrastructure project INOVA-OPTIMA SMIS code 49164, contract No. 658/2014, and the PROINSTITUTIO Project–contract No. 19PFE/17.10.2018 as well as the European Regional Development Fund through Competitiveness Operational Programme 2014-2020, Action 1.1.3 Creating synergies with H2020 Programme, project H2020 Support Centre for European project management and European promotion, MYSMIS code 107874 for funding. Aldo Di Carlo gratefully acknowledges the financial support from the Ministry of Science and Higher Education of the Russian Federation in the framework of MegaGrant (No. 075-15-2019-872 /074-02-2018-327). Antonio Agresti and Sara Pescetelli gratefully acknowledge funding from the European Union's Horizon 2020 Research Innovation Program under grant agreement graphene Core3 SGA881603. The research was conducted at the Tomsk Polytechnic University within the aid a Tomsk Polytechnic University- Competitiveness Enhancement Program grant.

Conflicts of Interest: The authors declare no conflict of interest in publishing this manuscript.

References

1. Trovó, A.G.; Nogueira, R.F.; Agüera, A.; Fernandez-Alba, A.R.; Sirtori, C.; Malato, S. Degradation of sulfamethoxazole in water by solar photo-Fenton. Chemical and toxicological evaluation. *Water Res.* **2009**, *43*, 3922–3931. [CrossRef] [PubMed]
2. Magureanu, M.; Piroi, D.; Mandache, N.B.; David, V.; Medvedovici, A.; Parvulescu, V.I. Degradation of pharmaceutical compound pentoxifylline in water by non-thermal plasma treatment. *Water Res.* **2010**, *44*, 3445–3453. [CrossRef] [PubMed]
3. Klavarioti, M.; Mantzavinos, D.; Kassinos, D. Removal of residual pharmaceuticals from aqueous systems by advanced oxidation processes. *Environ. Int.* **2009**, *35*, 402–417. [CrossRef] [PubMed]
4. Haber, F.; Weiss, J. The catalytic decomposition of hydrogen peroxide by iron salts. *Proc. R. Soc. Lond.* **1934**, *147*, 332–351. [CrossRef]
5. Stasinakis, A.S. Use of selected advanced oxidation processes (aops) for wastewater treatment-a mini review. *Glob. NEST J.* **2008**, *10*, 376–385.
6. Bankole, M.T.; Tijani, J.O.; Mohammed, I.A.; AbdulKareem, A.S. A review on nanotechnology as a tool of change in Nigeria. *Sci. Res. Essays* **2014**, *9*, 213–223.
7. Loures, C.C.; Alcântara, M.A.; Izário Filho, H.J.; Teixeira, A.C.; Silva, F.T.; Paiva, T.C.; Samanamud, G.R. Advanced Oxidative Degradation Processes: Fundamentals and Applications. *Int. Rev. Chem. Eng.* **2013**, *5*, 102–120. [CrossRef]
8. Gupta, S.B. Investigation of a Physical Disinfection Process Based on Pulsed Underwater Corona Discharges. Ph.D. Thesis, Forschungszentrum Karlshrue, Karlsruhe, Germany, 2007.
9. Esplugas, S.; Bila, D.M.; Krause, L.G.T.; Dezotti, M. Ozonation and advanced oxidation technologies to remove endocrine disrupting chemicals (EDCs) and pharmaceuticals and personal care products (PPCPs) in water effluents. *J. Hazard. Mater.* **2007**, *149*, 631–642. [CrossRef]
10. Iqbal, M.; Bhatti, I.A.; Ahmad, I. Photo-degradation of the methyl blue: Optimization through response surface methodology using rotatable center composite design. *Int. J. Basic Appl. Sci.* **2013**, *2*, 145. [CrossRef]
11. Rizzo, L.; Meric, S.; Guida, M.; Kassinos, D.; Belgiorno, V. Heterogenous photocatalytic degradation kinetics and detoxification of an urban wastewater treatment plant effluent contaminated with pharmaceuticals. *Water Res.* **2009**, *43*, 4070–4078. [CrossRef]
12. Soresa, M. Ayka Addis Textile Wastewater Treatment by the Fenton's Reagent. Addis Ababa University Institute of Technology School of Graduate Studies, Department of Chemical and Engineering, *A Thesis Submitted to the Graduate Studies of Addis Ababa University, in Partial Fulfillment of the Degree of Master of Science in Chemical Engineering* (Process Engineering). 2011. Available online: http://localhost:80/xmlui/handle/123456789/8575 (accessed on 1 June 2011).
13. Lin, Y.T.; Weng, C.H.; Chen, F.Y. Key operating parameters affecting photocatalytic activity of visible-light-induced C-doped TiO_2 catalyst for ethylene oxidation. *Chem. Eng. J.* **2014**, *248*, 175–183. [CrossRef]
14. Lazar, M.A.; Varghese, S.; Nair, S.S. Photocatalytic Water Treatment by Titanium Dioxide: Recent Updates. *Catalysts* **2012**, *2*, 572–601. [CrossRef]
15. Klaysri, R.; Ratova, M.; Praserthdam, P.; Kelly, P. Deposition of Visible Light-Active C-Doped Titania Films via Magnetron Sputtering Using CO_2 as a Source of Carbon. *Nanomaterials* **2017**, *7*, 113. [CrossRef]
16. Schäffer, J. Immobilization of TiO_2 Via Different Routes for Photocatalytic Reactions in a PDMS Based Microreactor. Bachelor's Thesis, University of Twente, Enschede, The Netherlands, 2012. Available online: http://purl.utwente.nl/essays/62126 (accessed on 1 August 2012).
17. Lindstrom, H.; Wootton, R.; Iles, A. High surface area titania photocatalytic microfluidic reactors. *AIChE J.* **2007**, *53*, 695–702. [CrossRef]
18. Shan, A.Y.; Ghazi, T.I.; Rashid, S.A. Immobilisation of titanium dioxide onto supporting materials in heterogeneous photocatalysis: A review. *Appl. Catal. A Gen.* **2010**, *389*, 1–8. [CrossRef]
19. Brinker, C.J.; Scherer, G.W. *Solgel Science: The Physics and Chemistry of Solgel Processing*; Academic Press Inc.: Cambridge, MA, USA, 1990; ISBN 0-12-134970-5.
20. Mechiakh, R.; Sedrine, N.B.; Chtourou, R.; Bensaha, R. Correlation between microstructure and optical properties of nano-crystalline TiO_2 thin films prepared by sol-gel dip coating. *Appl. Surf. Sci.* **2010**, *15*, 670–676. [CrossRef]

21. Avci, N.; Smet, P.F.; Poelman, H.; Van de Velde, N.; De Buysser, K.; Van Driessche, I.; Poelman, D. Characterization of TiO_2 powders and thin films prepared by non-aqueous sol-gel techniques. *J. SolGel Sci. Technol.* **2009**, *52*, 424–431. [CrossRef]
22. Calderon-Moreno, J.M.; Preda, S.; Predoana, L.; Zaharescu, M.; Anastasescu, M.; Nicolescu, M.; Stoica, M.; Stroescu, H.; Gartner, M.; Buiu, O.; et al. Effect of polyethylene glycol on porous transparent TiO_2 films prepared by sol-gel method. *Ceram. Int.* **2014**, *40*, 2209–2220. [CrossRef]
23. Aksoy, S.; Caglar, Y. Structural transformations of TiO_2 films with deposition temperature and electrical properties of nanostructure n-TiO_2/p-Si heterojunction diode. *J. Alloy. Compd.* **2014**, *613*, 330–337. [CrossRef]
24. Kumar, A.; Mondal, S.; Kumar, S.G.; Rao, K.K. High performance sol-gel spin-coated titanium dioxide dielectric based MOS structures. *Mater. Sci. Semicond. Process.* **2015**, *40*, 77–83. [CrossRef]
25. Shu, H.; Yang, M.; Liu, Q.; Luo, M. Study of TiO_2-Modified Sol Coating Material in the Protection of Stone-Built Cultural Heritage. *Coatings* **2020**, *10*, 179. [CrossRef]
26. Molkenova, A.; Khamkhash, L.; Zhussupbekova, A.; Zhussupbekov, K.; Sarsenov, S.; Taniguchi, I.; Shvets, I.V.; Atabaev, T.S. Solution-Based Deposition of Transparent Eu-Doped Titanium Oxide Thin Films for Potential Security Labeling and UV Screening. *Nanomaterials* **2020**, *10*, 1132. [CrossRef]
27. Saliba, M.; Matsui, T.; Seo, J.Y.; Domanski, K.; Correa-Baena, J.P.; Nazeeruddin, M.K.; Zakeeruddin, S.M.; Tress, W.; Abate, A.; Hagfeldt, A.; et al. Cesium-containing triple cation perovskite solar cells: Improved stability, reproducibility and high efficiency. *Energy Environ. Sci.* **2016**, *9*, 1989–1997. [CrossRef] [PubMed]
28. Polyakov, A.Y.; Smirnov, N.B.; Shchemerov, I.V.; Saranin, D.S.; Le, T.S.; Didenko, S.I.; Kuznetsov, D.V.; Agresti, A.; Pescetelli, S.; Matteocci, F.; et al. Trap states in multication mesoscopic perovskite solar cells: A deep levels transient spectroscopy investigation. *Appl. Phys. Lett.* **2018**, *113*, 263501. [CrossRef]
29. Agresti, A.; Pescetelli, S.; Najafi, L.; Castillo, A.D.; Oropesa-Nuñez, R.; Busby, Y.; Bonaccorso, F.; Di Carlo, A. Graphene and related 2D materials for high efficient and stable perovskite solar cells. In Proceedings of the IEEE 17th International Conference on Nanotechnology (IEEE-NANO), Pittsburgh, PA, USA, 25–28 July 2017; pp. 145–150. [CrossRef]
30. Agresti, A.; Cinà, L.; Pescetelli, S.; Taheri, B.; Di Carlo, A. Stability of dye-sensitized solar cell under reverse bias condition: Resonance Raman spectroscopy combined with spectrally resolved analysis by transmittance and efficiency mapping. *Vib. Spectrosc.* **2016**, *84*, 106–117. [CrossRef]
31. Busby, Y.; Agresti, A.; Pescetelli, S.; Di Carlo, A.; Noel, C.; Pireaux, J.J.; Houssiau, L. Aging effects in interface-engineered perovskite solar cells with 2D nanomaterials: A depth profile analysis. *Mater. Today Energy* **2018**, *9*, 1–10. [CrossRef]
32. Zhuang, J.; Dai, W.; Tian, Q.; Li, Z.; Xie, L.; Wang, J.; Liu, P.; Shi, X.; Wang, D. Photocatalytic degradation of RhB over TiO_2 bilayer films: Effect of defects and their location. *Langmuir* **2010**, *26*, 9686–9694. [CrossRef]
33. Chen, Y.; Stathatos, E.; Dionysiou, D.D. Microstructure characterization and photocatalytic activity of mesoporous TiO_2 films with ultrafine anatase nanocrystallites. *Surf. Coat. Technol.* **2008**, *202*, 1944–1950. [CrossRef]
34. Pelaez, M.; Falaras, P.; Likodimos, V.; Kontos, A.G.; Armah, A.; O'shea, K.; Dionysiou, D.D. Synthesis, structural characterization and evaluation of sol-gel-based NF-TiO_2 films with visible light-photoactivation for the removal of microcystin-LR. *Appl. Catal. B Environ.* **2010**, *99*, 378–387. [CrossRef]
35. Han, C.; Pelaez, M.; Likodimos, V.; Kontos, A.G.; Falaras, P.; O'Shea, K.; Dionysiou, D.D. Innovative visible light-activated sulfur doped TiO_2 films for water treatment. *Appl. Catal. B Environ.* **2011**, *107*, 77–87. [CrossRef]
36. Lu, P.J.; Chien, C.W.; Chen, T.S.; Chern, J.M. Azo dye degradation kinetics in TiO2film-coated photoreactor. *Chem. Eng. J.* **2010**, *163*, 28–34. [CrossRef]
37. Kenanakis, G.; Vernardou, D.; Dalamagkas, A.; Katsarakis, N. Photocatalytic and electrooxidation properties of TiO_2 thin films deposited by sol-gel. *Catalysis Today* **2015**, *240 Pt A*, 146–152. [CrossRef]
38. Zabihi, F.; Xie, Y.; Gao, S.; Eslamian, M. Morphology, conductivity, and wetting characteristics of PEDOT: PSS thin films deposited by spin and spray coating. *Appl. Surf. Sci.* **2015**, *338*, 163–177. [CrossRef]
39. Clausi, M.; Santonicola, M.G.; Laurenzi, S. Fabrication of carbon-based nanocomposite films by spin-coating process: An experimental and modeling study of the film thickness. *Compos. Part A Appl. Sci. Manuf.* **2016**, *88*, 86–97. [CrossRef]

40. Guillard, C.; Lachheb, H.; Houas, A.; Ksibi, M.; Elaloui, E.; Herrmann, J.M. Influence of chemical structure of dyes, of pH and of inorganic salts on their photocatalytic degradation by TiO_2 comparison of the efficiency of powder and supported TiO_2. *J. Photochem. Photobiol. A Chem.* **2003**, *158*, 27–36. [CrossRef]
41. Danish, M.; Ambreen, S.; Chauhan, A.; Pandey, A. Optimization and comparative evaluation of optical and photocatalytic properties of TiO_2 thin films prepared via sol-gel method. *J. Saudi Chem. Soc.* **2015**, *19*, 557–562. [CrossRef]
42. Dijkstra, M.F.; Panneman, H.J.; Winkelman, J.G.; Kelly, J.J.; Beenackers, A.A. Modeling the photocatalytic degradation of formic acid in a reactor with immobilized catalyst. *Chem. Eng. Sci.* **2002**, *57*, 4895–4907. [CrossRef]
43. Rajendran, K.; Kumar, V.S.; Rani, K.A. Synthesis and characterization of immobilized activated carbon doped TiO_2 thin films. *Optik Stuttgarter* **2014**, *125*, 1993–1996. [CrossRef]
44. Varshney, G.; Kanel, S.R.; Kempisty, D.M.; Varshney, V.; Agrawal, A.; Sahle-Demessie, E.; Varma, R.S.; Nadagouda, M.N. Nanoscale TiO_2 films and their application in remediation of organic pollutants. *Coord. Chem. Rev.* **2016**, *306 Pt 1*, 43–64. [CrossRef]
45. Arabatzis, I.M.; Antonaraki, S.; Stergiopoulos, T.; Hiskia, A.; Papaconstantinou, E.; Bernard, M.C.; Falaras, P. Preparation, characterization and photocatalytic activity of nanocrystalline thin film TiO_2 catalysts towards 3,5-dichlorophenol degradation. *J. Photochem. Photobiol. A Chem.* **2002**, *149*, 237–245. [CrossRef]
46. Jarka, P.; Tański, T.; Matysiak, W.; Krzemiński, Ł.; Hajduk, B.; Bilewicz, M. Manufacturing and investigation of surface morphology and optical properties of composite thin films reinforced by TiO_2, Bi_2O_3 and SiO_2 nanoparticles. *Appl. Surf. Sci.* **2017**, *424 Pt 2*, 206–212. [CrossRef]
47. Agresti, A.; Pescetelli, S.; Palma, A.L.; Martín-García, B.; Najafi, L.; Bellani, S.; Moreels, I.; Prato, M.; Bonaccorso, F.; Di Carlo, A. Two-dimensional (2D) Material Interface Engineering for Efficient Perovskite Large-area Modules. *ACS Energy Lett.* **2019**, *4*, 1862–1871. [CrossRef]
48. Palma, A.L.; Matteocci, F.; Agresti, A.; Pescetelli, S.; Calabrò, E.; Vesce, L.; Christiansen, S.; Schmidt, M.; Di Carlo, A. Laser-Patterning Engineering for Perovskite Solar Modules with 95% Aperture Ratio. *IEEE J. Photovolt.* **2017**, *7*, 1674–1680. [CrossRef]
49. Zanotti, G.; Angelini, N.; Mattioli, G.; Paoletti, A.M.; Pennesi, G.; Caschera, D.; Sobolev, A.P.; Beverina, L.; Calascibetta, A.M.; Sanzone, A.; et al. [1]Benzothieno[3,2-b][1]benzothiophene-Phthalocyanine Derivatives: A Subclass of Solution-Processable Electron-Rich Hole Transport Materials. *ChemPlusChem* **2020**. [CrossRef]
50. Agresti, A.; Pescetelli, S.; Palma, A.L.; Del Rio Castillo, A.E.; Konios, D.; Kakavelakis, G.; Razza, S.; Cinà, L.; Kymakis, E.; Bonaccorso, F.; et al. Graphene Interface Engineering for Perovskite Solar Module: A Power Conversion Efficiency Exceeding 12.5% over 50 cm^2 Active Area. *ACS Energy Lett.* **2017**, *2*, 279–287. [CrossRef]
51. Taheri, B.; Nia, N.Y.; Agresti, A.; Pescetelli, S.; Ciceroni, C.; Castillo, A.E.; Cinà, L.; Bellani, S.; Bonaccorso, F.; Di Carlo, A. Graphene-engineered automated sprayed mesoscopic structure for perovskite device scaling-up. *2D Mater.* **2018**, *5*, 045034. [CrossRef]
52. O'keeffe, P.; Catone, D.; Paladini, A.; Toschi, F.; Turchini, S.; Avaldi, L.; Martelli, F.; Agresti, A.; Pescetelli, S.; Del Rio Castillo, A.E.; et al. Supporting information graphene-induced improvements of perovskite solar cell stability: Effects on hot-carriers. *Nano Lett.* **2019**, *19*, 684–691. [CrossRef]
53. Agresti, A.; Pazniak, A.; Pescetelli, S.; Di Vito, A.; Rossi, D.; Pecchia, A.; der Maur, M.A.; Liedl, A.; Larciprete, R.; Kuznetsov, D.V.; et al. Titanium-carbide MXenes for work function and interface engineering in perovskite solar cells. *Nat. Mater.* **2019**, *18*, 1228–1234. Available online: www.nature.com/naturematerials (accessed on 14 October 2019). [CrossRef]
54. Najafi, L.; Taheri, B.; Martín-García, B.; Bellani, S.; Di Girolamo, D.; Agresti, A.; Oropesa-Nunez, R.; Pescetelli, S.; Vesce, L.; Calabro, E.; et al. MoS_2 Quantum Dot/Graphene Hybrids for Advanced Interface Engineering of CH_3NH_3 PbI_3 Perovskite Solar Cell with Efficiency over 20%. *ACS Nano* **2018**, *12*, 10736–10754. [CrossRef]
55. Wu, C.-Y.; Lee, Y.-L.; Lo, Y.-S.; Lin, C.-J.; Wu, C.-H. Thickness-dependent photocatalytic performance of nanocrystalline TiO_2 thin films prepared by sol–gel spin coating. *Appl. Surf. Sci.* **2013**, *280*, 737–744. [CrossRef]
56. Lin, H.-J.; Yang, T.-S.; Hsi, C.-S.; Wang, M.-C.; Lee, K.-C. Optical and photocatalytic properties of Fe^{3+}-doped TiO_2 thin films prepared by a sol–gel spin coating. *Ceram. Int.* **2014**, *40*, 10633–10640. [CrossRef]

57. Bsiri, N.; Zrir, M.A.; Bardaoui, A.; Bouaïcha, M. Morphological, structural and ellipsometric investigations of Cr doped TiO_2 thin films prepared by sol–gel and spin coating. *Ceram. Int.* **2016**, *42*, 10599–10607. [CrossRef]
58. Bamoulid, L.; Benoit-Marquié, F.; Aries, L.; Guenbour, A.; Bachir, A.B.; Maurette, M.T.; Ansart, F.; El Hajjaji, S. Investigations on composition and morphology of electrochemical conversion layer/titanium dioxide deposit on stainless steel. *Surf. Coat. Technol.* **2006**, *201*, 2791–2795. [CrossRef]
59. Chen, Y.; Dionysiou, D.D. Cor relation of structural properties and film thickness to photocatalytic activity of thick TiO_2 films coated on stainless steel. *Appl. Catal. B: Environ.* **2006**, *69*, 24–33. [CrossRef]
60. Khanna, S.; Marathey, P.; Chaliyawala, H.; Rajaram, N.; Roy, D.; Banerjee, R.; Mukhopadhyay, I. Fabrication of long-ranged close-packed monolayer of silica nanospheres by spin coating. *Colloids Surf. A* **2018**, *553*, 520–527. [CrossRef]
61. Wang, Q.; Juarez-Perez, E.J.; Jiang, S.; Qiu, L.; Ono, L.K.; Sasaki, T.; Wang, X.; Shi, Y.; Zheng, Y.; Qi, Y.; et al. Spin-Coated Crystalline Molecular Monolayers for Performance Enhancement in Organic Field-Effect Transistors. *J. Phys. Chem. Lett.* **2018**, *9*, 1318–1323. [CrossRef] [PubMed]
62. Wang, H.; Wang, Y.; Chen, X. Synthesis of uniform silver nanowires from AgCl seeds for transparent conductive films via spin-coating at variable spin-speed. *Colloids Surf. A* **2019**, *565*, 154–161. [CrossRef]
63. Gültekin, A.; Karanfil, G.; Özel, F.; Kuş, M.; Say, R.; Sönmezoğlu, S. Synthesis and characterisations of Au-nanoparticle-doped TiO_2 and CdO thin films. *J. Phys. Chem. Solids* **2014**, *75*, 775–781. [CrossRef]
64. Manley, E.F.; Strzalka, J.; Fauvell, T.J.; Jackson, N.E.; Leonardi, M.J.; Eastham, N.D.; Marks, T.J.; Chen, L.X. In Situ GIWAXS Analysis of Solvent and Additive Effects on PTB7 Thin Film Microstructure Evolution during Spin Coating. *Adv. Mater.* **2017**, *29*, 1703933. [CrossRef]
65. Chen, J.; Zhang, L.; Jiang, X.; Gao, K.; Liu, F.; Gong, X.; Chen, J.; Cao, Y. Using *o*-Chlorobenzaldehyde as a Fast Removable Solvent Additive during Spin-Coating PTB7-Based Active Layers: High Efficiency Thick-Film Polymer Solar Cells. *Adv. Energy Mater.* **2016**, *7*, 1601344. [CrossRef]
66. Wang, Q.; Zheng, X.; Deng, Y.; Zhao, J.; Chen, Z.; Huang, J. Stabilizing the α-Phase of $CsPbI_3$ Perovskite by Sulfobetaine Zwitterions in One-Step Spin-Coating Films. *Joule* **2017**, *1*, 371–382. [CrossRef]
67. Deora, M.S.; Sharma, S.K. Effect of incorporation of sulphur on the structural, morphological and optical studies of CdSe thin films deposited by solution processed spin coating technique. *Thin Solid Film.* **2019**, *670*, 68–75. [CrossRef]
68. Gültekin, A.; Karanfil, G.; Özel, F.; Kuş, M.; Say, R.; Sönmezoğlu, S. The influence of CdS quantum dots incorporation on the properties of CdO thin films. *Eur. Phys. J. Appl. Phys.* **2013**, *64*, 30303. [CrossRef]
69. Pérez, J.B.; Courel, M.; Pal, M.; Delgado, F.P.; Mathews, N.R. Effect of ytterbium doping concentration on structural, optical and photocatalytic properties of TiO_2 thin films. *Ceram. Int.* **2017**, *43*, 15777–15784. [CrossRef]
70. Hassan, M.E.; Cong, L.; Liu, G.; Zhu, D.; Cai, J. Synthesis and characterization of C-doped TiO2 thin films for visible-light-induced photocatalytic degradation of methyl orange. *Appl. Surf. Sci.* **2014**, *294*, 89–94. [CrossRef]
71. Massima Mouele, E.S.; Tijani, J.; Masikini, M.; Fatoba, O.; Eze, C.P.; Onwordi, C.T.; Zar Myint, M.T.; Kyaw, H.H.; Al-Sabahi, J.; Al-Abri, M.; et al. Spectroscopic Measurements of Dissolved O_3, H_2O_2 and OH Radicals in Double Cylindrical Dielectric Barrier Discharge Technology: Treatment of Methylene Blue Dye Simulated Wastewater. *Plasma* **2020**, *3*, 59–91. [CrossRef]
72. Boro, B.; Gogoi, B.; Rajbongshi, B.M.; Ramchiary, A. Nano-structured TiO_2/ZnO nanocomposite for dye-sensitized solar cells application: A review. *Renew. Sustain. Energy Rev.* **2018**, *81*, 2264–2270. [CrossRef]
73. Gupta, A.; Sahu, K.; Dhonde, M.; Murty, V.V. Novel synergistic combination of Cu/S co-doped TiO_2 nanoparticles incorporated as photo anode in dye sensitized solar cell. *Sol. Energy* **2020**, *203*, 296–303. [CrossRef]
74. Zhao, Y.; Han, Z.; Zhou, W.; Li, Q.; Fu, R.; Yu, D.; Zhao, Q. Water-Based TiO_2 Nanocrystal as an Electronic Transport Layer for Operationally Stable Perovskite Solar Cells. *Sol. RRL* **2019**, *3*, 1900167. [CrossRef]
75. Dubey, R.S.; Krishnamurthy, K.V.; Singh, S. Experimental studies of TiO2 nanoparticles synthesized by sol-gel and solvothermal routes for DSSCs application. *Results Phys.* **2019**, *14*, 102390. [CrossRef]
76. Wannaborworn, M.; Praserthdam, P.; Jongsomjit, B. A comparative study of solvothermal and sol-gel-derived nanocrystalline alumina catalysts for ethanol dehydration. *J. Nanomater.* **2015**, *2015*, 519425. [CrossRef]

77. Que, Y.P.; Weng, J.; Hu, L.H.; Wu, J.H.; Dai, S.Y. High open voltage and superior light-harvesting dye-sensitized solar cells fabricated by flower-like hierarchical TiO_2 composed with highly crystalline nanosheets. *J. Power Sources* **2016**, *307*, 138–145. [CrossRef]
78. Senthil, T.S.; Kim, D.; Muthukumarasamy, N.; Kang, M. Closely packed dense network rutile nanorods with gadolinium for efficient dye sensitized solar cells. *Appl. Surf. Sci.* **2014**, *313*, 858–863. [CrossRef]
79. Li, J.; Zhang, H.; Wang, W.; Qian, Y.; Li, Z. Improved performance of dye-sensitized solar cell based on TiO_2 photoanode with FTO glass and film both treated by $TiCl_4$. *Phys. B Condens. Matter* **2016**, *500*, 48–52. [CrossRef]
80. Dong, Y.X.; Wang, X.L.; Jin, E.M.; Jeong, S.M.; Jin, B.; Lee, S.H. One-step hydrothermal synthesis of Ag decorated TiO_2 nanoparticles for dye-sensitized solar cell application. *Renew. Energy* **2019**, *135*, 1207–1212. [CrossRef]
81. Ramakrishnan, V.M.; Natarajan, M.; Santhanam, A.; Asokan, V.; Velauthapillai, D. Size controlled synthesis of TiO_2 nanoparticles by modified solvothermal method towards effective photo catalytic and photovoltaic applications. *Mater. Res. Bull.* **2018**, *97*, 351–360. [CrossRef]
82. Gesesse, G.D.; Li, C.; Paineau, E.; Habibi, Y.; Remita, H.; Colbeau-Justin, C.; Ghazzal, M.N. Enhanced Photogenerated Charge Carriers and Photocatalytic Activity of Biotemplated Mesoporous TiO_2 Films with a Chiral Nematic Structure. *Chem. Mater.* **2019**, *31*, 4851–4863. [CrossRef]
83. Wu, M.; Lin, G.; Chen, D.; Wang, G.; He, D.; Feng, S.; Xu, R. Sol hydrothermal synthesis and hydrothermally structural evolution of nanocrystal titanium dioxide. *Chem. Mater.* **2002**, *14*, 1974–1980. [CrossRef]
84. Wei, J.; Wen, X.; Zhu, F. Influence of surfactant on the morphology and photocatalytic activity of anatase TiO_2 by solvothermal synthesis. *J. Nanomater.* **2018**, *2018*, 3086269. [CrossRef]